This article has been accepted for publication in a future issue of this journal, but has not been fully edited. Content may change prior to final publication. Citation information: DOI 10.1109/JRFID.2020.3041419, IEEE Journal of Radio Frequency Identification

A Phase-based Ranging Method for Long-range RFID Positioning with Quantum Tunneling Tags

Cheng Qi, *Student Member, IEEE,* Francesco Amato, *Member, IEEE,*
Mohammad Alhassoun, *Member, IEEE,* and Gregory D. Durgin, *Senior Member, IEEE*

***Abstract*—This work demonstrates the ability to extend the positioning range of low-powered RFID tags to distances usually not achievable with other wireless or conventional RFID technologies. The technique is performed through a Received Signal Phase (RSP)-based method on a 5.8 GHz backscatter tunneling tag, in multipath-rich indoor and outdoor environments, at distances up to 35 meters from the reader. Distance errors as low as 0.1% of the total reader-to-tag distance were observed with average errors of 0.8% and 0.6% for indoor and outdoor environments, respectively. Compared to Received Signal Strength (RSS)-based techniques, the average distance estimation accuracy is improved by a factor of 51 and 38 for indoor and outdoor environments, respectively. Moreover, an Effective Isotropic Radiated Power (EIRP) of only 10.5 dBm and a biasing power for the tunneling tag of only 21.3 μW at 80 mV promise a low-power, long-range sub-meter scale positioning technique with a projected maximum range over 1 km.**

***Index Terms*—RFID; Localization; Tracing; Fine-scale Positioning; Long-range Backscattering; Tunneling Tag; IoT**

I. Introduction

The rapid development of the Internet-of-Things and RFID industry is witnessing an increasing demand for systems that can identify people and objects together with their locations. A highly accurate wireless positioning system, in fact, could revolutionize smartphone applications, augmented reality experiences, and autonomous vehicle navigation with the RFID technology being the key player in their development. In fact, RFID readers perform coherent detection that allows to gather both Received Signal Strengths (RSS), and coherent Received Signal Phases (RSP) that can be used to locate and track an RFID tag. Yet, fundamental limitations in wireless localization and positioning techniques remain: fine-scale accuracy, particularly at the fringe of coverage for both short- and long-range radios, is extremely difficult to achieve. Multiple factors affect the coverage and the accuracy of localization: the frequency bandwidth used by the RFID system, the sensitivity of the RFID reader, the antenna gain, the localization techniques, the environmental factors, the availability of clear line-of-sight (LoS) between tags and readers, multipath, and propagation losses.

Starting from early results described in [1], this paper presents how to break the range limit of RFID positioning by combining received signal phase (RSP)-based positioning methods with tunneling tags. It exploits both the full-coherent signal and the multiple phase data that a single RFID reader receives from a tag operating at the 5.8 GHz industrial-scientific-medical (ISM) band (5.725 GHz to 5.975 GHz). A tunneling tag amplifies the signal strength of a backscattered signal and preserves its phase allowing for accurate estimates of position and/or orientation at long distances. Through both indoor and outdoor reader-to-tag distance measurements, this article demonstrates how long-range LoS positioning is possible with tunneling tags; it compares the achieved accuracy with that of a conventional RSS-based technique; and it introduces an effective calibration method that can further increase the accuracy. Finally, all the results obtained with the tunneling tag (TT) are compared with those achieved through a conventional Semi-passive tag (SpT).

With respect to the state-of-the-art of RFID positioning systems (summarised in Fig. 1 and discussed in Sec. II-A), the proposed technology gives lower positioning errors (below 0.8%) than state-of-the art solutions at above-average backstttering ranges (35 meters, and more). Traditional positioning techniques tend to have percentage distance errors that worsen when the ranges increase. With this work, instead, the lowest

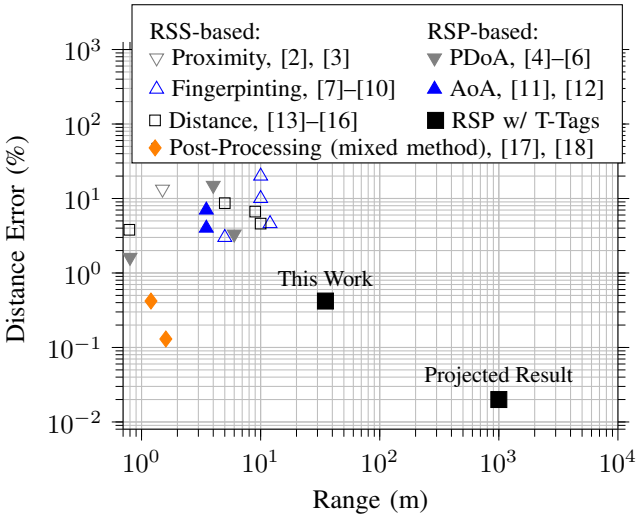

Fig. 1: RFID positioning and tracking techniques, state-of-the-art and prediction of what will be obtained by combining Tunneling Tags (TT) and RSP-based positioning approaches (discussed in Sec. V-C). Comparisons were made in terms of reported distance errors and maximum ranges.

C. Qi and G. D. Durgin are with the Propagation Group, Department of Electrical and Computer Engineering, Georgia Institute of Technology, Atlanta, USA (e-mail: cqi9@gatech.edu); F. Amato is with the Pervasive Electromagnetic Lab, Department of Civil and Computer Science Engineering, University of Roma Tor Vergata, Rome, Italy (f.amato@ieee.org); M. Alhassoun is with Electrical Engineering Department, King Fahd University of Petroleum and Minerals, Dhahran, Saudi Arabia.

This article has been accepted for publication in a future issue of this journal, but has not been fully edited. Content may change prior to final publication. Citation information: DOI 10.1109/JRFID.2020.3041419, IEEE Journal of Radio Frequency Identification

percentage errors are reported despite longer distances are involved.

Since multiple readers can be used for accurate positioning applications both in 2- and 3-dimensional spaces, this new technique enables real-time, low-powered, and long-range precise positioning of objects such as pallets, vehicles, animals, and goods. For instance, RFID readers equipped in smart warehouses could monitor goods while handling ground traffic of forklifts and staff equipped with tunneling tags. Finally, by operating at microwave frequencies, this system could be integrated within handheld devices or drones and communicate with future 5G networks.

II. Rationale

A. State of the Art

RFID positioning and tracking systems can be divided into different techniques based on their characteristics and approaches [19]. A summary of the state-of-the-art is shown in Fig. 1 where the errors (in %) are calculated as the ratio between the mean error at the maximum distance and the maximum distance itself[1]. The most common RFID positioning and tracking systems estimate the reader-to-tag distances using the RSS. They are classified into proximity-based techniques [2], [3]; RF-fingerprint techniques [7]–[10]; and distance-based techniques [13]–[16]. However, RSS-based methods suffer from poor accuracy, especially when the target is far away from the reader, therefore, shorter reading range means denser readers in the same experimental setup.

Researchers have proposed RSP-based methods to achieve higher accuracy. It has been shown in [4], [5], [20], [21] that phase-based spatial identification of RFID tags is feasible through a frequency domain phase difference of arrival (FD-PDoA) method, which is similar to frequency modulated continuous wave radars (FMCW) [4]. Nikitin, *et al.* demonstrated three techniques based on phase difference of arrival (TD-PDoA, FD-PDoA, and SD-PDoA) in [20], providing simulation results for a simple modeling example of a tag moving by a pair of reader antennas in the presence of multipath. Zhou, *et al.* tracked the location of moving backscatter RF tags and achieved a range error of approximately 1 mm by using a composite dual-frequency continuous-wave and continuous-wave (DFCW/CW) radar system based on a custom 5.8 GHz backscatter RFID system in a typical indoor laboratory environment in LoS [5], [21]. Researchers in [6] presented a sensor fusion approach that combines the phase-based localization method with data acquired by kinematic sensors for mobile nodes equipped with a UHF RFID system.

Angle-of-arrival (AoA) techniques also utilize RSP, allowing RFID of readers with active antenna arrays to find the direction of arrival of the incident wave [11], [12]. Assisted techniques utilize various information and post-processing such as Hybrid Inertial Microwave Reflectometry (HIMR) algorithm [17], Kalman filtering [18], and machine learning to provide accurate location estimates in real-time.

[1]When this mean error is not reported, an average error is calculated among all the achieved distances.

Although researches have improved the accuracy, few techniques have been proposed to improve ditance estimation accuracy at long distances. Many researchers have built RSS-based or RSP-based location tracking systems at higher frequency bands (e.g., 5.8 GHz) to achieve higher accuracy brought by the shorter wavelength and broader bandwidth. Nonetheless, higher frequencies bring shorter communication ranges due to the higher path loss. Therefore, positioning an RFID tag with both high accuracy and at a long distance in a multipath-rich environment remains a challenging task. In the last few years, researchers have proposed solutions to overcome the range limits of passive and semi-passive RFID tags [22], [23]. Experimental results in [24] have shown how a 5.8 GHz RFID tunneling tag can significantly increase the range of backscatter radio links while consuming very low power. Authors in [23], [25]–[27] have suggested equipping RFID tags with Van Atta-based Arrays [28] to further increase the communication range while maintaining a wide field-of-view.

B. The Tunneling Effect

The well known link budget equation of a backscattering system:

$$P_r = P_T G_{tx} G_{rx} G_t^2 \left(\frac{\lambda}{4\pi d}\right)^4 M, \tag{1}$$

can involve one tag with gain G_t, and one co-located bistatic reader with transmitting and receiving antenna gains G_{tx} and G_{rx}, respectively [29]. It suggests that a system engineer can operate on some parameters to improve the reading distance d between the reader and the transponder. For example, a modulation factor $M = \frac{1}{4}\left|\Gamma_1 - \Gamma_2\right|^2$ [29] can achieve values greater than 1 when active loads are used. In particular, a tunneling reflection amplifier based on tunnel diodes and mounted on a tunneling tag (Fig. 2, [22]) is an efficient way to obtain a modulation factor $M > 1$ with very low biasing power (21.32 μW at 80 mV [1]). The tunneling tag exploits the *tunneling effect* that, as shown in the region **I** of Fig. 2b, takes place for extremely low reverse and forward biasing voltages applied to a tunnel diode. When the forward biasing voltage slightly increases, the tunneling effect fades and the the device displays a negative resistance $-R_L$. The corresponding amplitude of the reflection coefficient $|\Gamma| = \left|\frac{Z_L - Z_{ant}}{Z_L + Z_{ant}^*}\right| = \frac{-R_L - Z_{ant}}{-R_L + Z_{ant}^*}$ can be made greater than one ($|\Gamma| > 1$, hence $M > 1$) by matching the value of $-R_L$ with a properly matched antenna impedance Z_{ant}. Therefore, the on/off biasing of the tunneling diode can modulate, backscatter, and amplify an impinging RF signal and enhance the backscattering link range.

C. RSP-based Distance Estimation

The coherent detection performed by RFID readers allows the recovery of both amplitudes and phases of the received signals to perform spatial identification, such as FD-PDoA, of an RFID tag. Upon demodulation and after filtering out the DC component of a backscattered RFID signal (Fig. 3), the RSS and the RSP can be expressed as:

$$P_{RSS} = \frac{I_{rx}^2 + Q_{rx}^2}{Z_0}, \tag{2}$$

This article has been accepted for publication in a future issue of this journal, but has not been fully edited. Content may change prior to final publication. Citation information: DOI 10.1109/JRFID.2020.3041419, IEEE Journal of Radio Frequency Identification

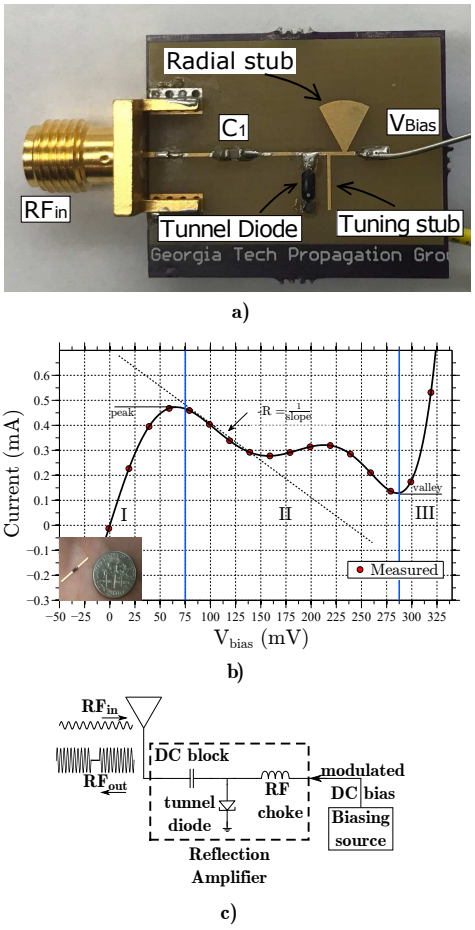

Fig. 2: a) Microstrip line structure of the tunneling reflection amplifier as in [30]; b) the measured IV curve [22] of tunnel diode model MBD5057 c) The block diagram of the tunneling tag.

$$\varphi_{RSP} = \arctan\left(\frac{Q_{rx}}{I_{rx}}\right) \in [0, 2\pi), \tag{3}$$

where I_{rx} and Q_{rx} are the amplitudes of the in-phase (I) and quadrature (Q) channels of the received signal; and Z_0 is the input impedance of the receiving antenna (50 Ω).

In free space, when no multipath reflections occur, the unwrapped phase offset φ_{ps} caused by the LoS round-trip propagation can be written as [20]:

$$\varphi_{ps} = -\frac{4\pi f_c d}{c}, \tag{4}$$

where c is the speed of light in free-space; d is the distance between the reader and the target tag; and f_c is the carrier frequency of the RFID reader.

The overall φ_{RSP} in (3) with presence of multipath can then be expressed also as:

$$\varphi_{RSP}(f_c) = \varphi_{ps}(f_c) + \varphi_0(f_c) + \varphi_m(f_c) + \varphi_t, \tag{5}$$

where the dependency on the carrier frequency f_c is highlighted. In (5), φ_0 is the phase offset caused by the system and due to cables, antennas, tag modulation, and other reader components; φ_m is the phase offset caused by the multipath channel; and φ_t is the phase error due to the thermal noise, the local oscillator (LO), the IQ imbalance, the transmit-to-receive leakage [31], and other random interference such as a person passing by.

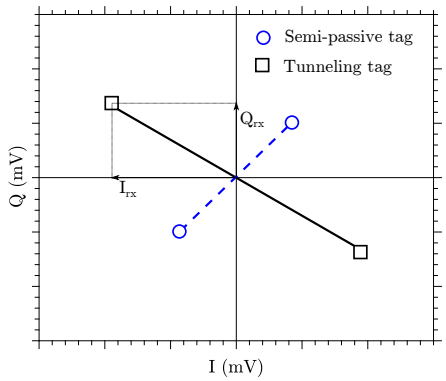

Fig. 3: Received signal from Semi-passive and Tunneling Tags.

An RSP-based method [5] can be used to estimate the distance $\hat{d}$ between a reader and a tag. The method consists in subtracting the phases, φ_{RSP}, of two signals received at two adjacent frequency channels and in averaging those differences over a specific band:

$$\hat{d} = \frac{c}{4\pi N}\sum_{n=1}^{N-1}\left|\frac{\varphi_{RSP_n} - \varphi_{RSP_{n+1}}}{f_n - f_{n+1}}\right|. \tag{6}$$

With φ_{RSP_n} and $\varphi_{RSP_{n+1}}$ being the measured phases of the received signals obtained through (3) at the reader carrier frequencies f_n and f_{n+1}, respectively; and N being the number of the frequency channels.

Through a uniform frequency step $\Delta f = f_{n+1} - f_n$, the equivalent wave length $\lambda_e = \frac{c}{\Delta f}$ can be defined. Therefore, (6) becomes:

$$\hat{d} = \frac{\lambda_e}{4\pi N}\sum_{n=1}^{N-1}\left|\varphi_{RSP_n} - \varphi_{RSP_{n+1}}\right| = \frac{\lambda_e}{4\pi}\overline{\Delta\varphi}, \tag{7}$$

with

$$\overline{\Delta\varphi} = \frac{1}{N}\sum_{n=1}^{N-1}\left|\varphi_{RSP_n} - \varphi_{RSP_{n+1}}\right|, \tag{8}$$

being the average phase offset caused by both the system and by the multipath environment. Since the received wrapped signal phase φ_{RSP} is equal to the unwrapped phase φ_{ps} only when $\left|\varphi_{RSP_n} - \varphi_{RSP_{n+1}}\right| \geq 2\pi$, then, the maximum detection range $\hat{d}_{max}$ of the phase-based method is determined by the minimum frequency step Δf of the reader:

$$\hat{d}_{max} = \frac{c}{2\Delta f} = \frac{\lambda_e}{2}. \tag{9}$$

Although most conventional positioning techniques for RFID tags use distance-dependent path loss models based on RSS, they are usually severely affected by both the propagation environment and the properties of the tagged objects. Therefore, RSS-based positioning techniques cannot be universally applied, and absolute calibration is rather difficult. Moreover,

unlike a conventional backscatter RFID tag that has a constant modulation factor M, the gain of the tunneling tag fluctuates between 5 dB to 38 dB for impinging powers ranging between -55 dBm and -80 dBm [24], respectively. The nonlinear relationship between the gain and the impinging power makes the calibration of RSS-based localization for tunneling tag even more difficult. However, the phase offset of the backscatter signal caused by the tunneling tag modulation is a constant that is independent of the impinging power and does not affect phase-based positioning techniques.

D. Distance and Error Estimation

To achieve good accuracy, system calibration is usually necessary for most positioning techniques before performing any measurements. For the RSP-based method, the ground-truth distance d between a reader and a tag is affected by distance errors ϵ such that the estimated distance $\hat{d}$ in (7):

$$\hat{d} = d + \epsilon, \tag{10}$$

includes the distance errors ϵ:

$$\hat{d} = d + \epsilon_0 + \epsilon_m + \epsilon_t; \tag{11}$$

where ϵ_0 is the distance error brought by the phase delay due to wave traveling within the RF cables and traces in the reader and tag; ϵ_m is the error brought by multipath; and ϵ_t is the error due to the thermal noise, the phase noise of the LO, the IQ imbalance, the transmit-to-receive leakage [31], and other interference sources such as a person passing by. Finally, by comparing the ground-truth distance d with the estimated $\hat{d}$, it is possible to define the percentage error as:

$$\epsilon_{\%} = \frac{\hat{d} - d}{d} \cdot 100\% \tag{12}$$

III. Multipath

A. Multipath Channel Modeling

Any terrestrial, non-laboratory radio channel will contain multipath components due to the reflection, diffraction, and scattering of electromagnetic waves. Multipath introduces numerous delayed copies of the original signal, which distort time-of-flight measurements. Wireless engineers often model the multipath channel as a collection of discrete multipath components constituting a *power delay profile*, $p(\tau)$, as a function of delay τ:

$$p(\tau) = \sum_i p_i \delta(\tau - \tau_i) \approx \frac{P_o}{\sigma_{\text{RMS}}} \exp\left(-\frac{\tau}{\sigma_{\text{RMS}}}\right) \mathrm{u}(\tau) \tag{13}$$

where p_i is the power of the ith multipath component, arriving at delay τ_i, $\mathrm{u}(\tau)$ is the unit step function. Delays for this analysis have been normalized relative to the first arriving multipath component at $\tau = 0$. The power delay profile generally consists of a first-arriving LoS component that also is usually the strongest in terms of power. Subsequent components generally, but not strictly, decay as the arrival time increases its delay. For this reason, radio engineers early capture the overall shape of typical power delay profiles with an exponential distribution of power *vs* delay, as indicated in (13), which depends only on the root-mean-squared (RMS) delay spread, σ_{RMS} [32].

The exponential model for power-delay-profile is a helpful guide for the dispersive nature of a radio channel. The RMS delay spread, in particular, is often enough to completely characterize the *coherence bandwidth* of a radio channel – the bandwidth over which the channel appears essentially "flat". For an exponentially decaying distribution of power in delay, the mean delay (as referenced from $\tau = 0$ in (13)) *and* the RMS width (second centered moment) of the distribution are both given by σ_{RMS}. RMS delay spread has been measured extensively for indoor and outdoor one-way channels and is typically calculated from spatial-averaging of at least several, local area power impulse responses to remove small-scale fading effects.

If the beginning of a power delay profile marks the arrival of a first LoS component, then the absolute delay of this first component can be used for precise positioning. However, if a narrowband signal is probing the channel phase as a function of frequency, then *all* multipath components will contribute to this aggregate measurement – not simply the first arriving component. Thus, we would expect the *centroid* of the distribution to introduce a consistent bias in phase change as a function of frequency (causing a positioning algorithm to *overestimate* the distance between transmitter and receiver). Likewise, the *RMS width* (delay spread) of the distribution will influence the variability of instantaneous phase measurements about the average, biased range estimate.

For the purposes of backscatter positioning with narrowband phase measurements, we should not simply consider the 1-way power delay profile. First, it is more natural to measure an *envelope profile* in signal processing with units proportional to *voltage* rather than power. Fortunately, the envelope distribution of the one-way channel should follow naturally from the square root of the power delay profile and will also be exponential. The centroid and RMS width of the envelope profile will differ, though, as summarized in Tab. I.

TABLE I: Idealized centroids and RMS widths of multipath distributions in delay for one- and two-way channels, with power or envelope delay spectra.

Delay Spec.	Profile, $\tau > 0$	Centroid	RMS Width
1-way Power	$\frac{\exp\left(\frac{-\tau}{\sigma_{\text{RMS}}}\right)}{\sigma_{\text{RMS}}}$	σ_{RMS}	σ_{RMS}
1-way Env.	$\frac{\exp\left(\frac{-\tau}{2\sigma_{\text{RMS}}}\right)}{2\sigma_{\text{RMS}}}$	$2\sigma_{\text{RMS}}$	$2\sigma_{\text{RMS}}$
2-way Power	$\frac{\tau^2 \exp\left(\frac{-\tau}{\sigma_{\text{RMS}}}\right)}{2\sigma_{\text{RMS}}^3}$	$3\sigma_{\text{RMS}}$	$\sqrt{3}\sigma_{\text{RMS}}$
2-way Env.	$\frac{\tau \exp\left(\frac{-\tau}{2\sigma_{\text{RMS}}}\right)}{4\sigma_{\text{RMS}}^2}$	$4\sigma_{\text{RMS}}$	$2\sqrt{2}\sigma_{\text{RMS}}$

If the radio channel is measured in a simple, monostatic backscatter configuration, the radio signal must travel through the channel twice. For a single-antenna RFID tag with load modulation, the effective channel is the *convolution* of a one-way channel with itself. A channel that follows a conventional exponential decay of power as a function of delay will have

This article has been accepted for publication in a future issue of this journal, but has not been fully edited. Content may change prior to final publication. Citation information: DOI 10.1109/JRFID.2020.3041419, IEEE Journal of Radio Frequency Identification

an envelope spectrum of the generic form $\tau \exp(-\tau)$ in the two-way link. Furthermore, the power delay spectrum of the two-way link would naturally follow the square of the envelope delay spectrum, leading to a generic $\tau^2 \exp(-\tau)$ distribution. Tab. I contains the profile shape for each type of spectrum and link, with the appropriate scaling constants to normalize the area under the distribution to 1.

The fine structure of the discrete multipath channel model will cause deviations from the ideal centroids and RMS widths of Tab. I. Even ignoring this complexity, a conventional RMS delay spread of σ_{RMS}, could reasonably lead to 1, 2, 3, or 4 times the actual offset error, depending on how the radio channel is measured and processed. The preliminary measurements and analysis in this paper use the centroid error corresponding to the two-way channel envelope profile. This appears to match the error best for the specific, measured backscatter links.

B. Evidence of Multipath Channel

Indoor settings are characterized by a multipath-rich environment where the φ_m in (5) contributes significantly to the measured phase φ_{RSP} and may significantly affect the correct estimation of the actual tag position, especially at short distances. To calibrate out the error added by the multipath propagation (ϵ_m), the multipath-rich wireless channel is investigated by using the setup shown in the inset of Fig. 4 having two antennas at a distance of 3 m from each other. Both the reader and the tag antennas were connected to a vector network analyzer (VNA) to record the S-parameters and measure the channel frequency response from 4.8 GHz to 6.8 GHz. The 2-way envelope delay spectrum of the multipath channel can be derived by:

$$P_{rx}(\tau) = \int_{-\infty}^{+\infty} S_{21}(f) S_{12}(f) e^{2j\pi f \tau} df, \tag{14}$$

where $P_{rx}(\tau)$ is the magnitude of the 2-way envelope delay spectrum. Five measurements were taken to average out the impact of small scale fading whose effect is depicted by the solid line in Fig. 4.

In Fig. 4 both the LoS and the multipath components that generate the delay profile of an indoor environment are highlighted. To obtain a high-resolution multipath channel model required for an accurate estimation of tag location, a deconvolution algorithm, called the CLEAN algorithm [33]–[35] was used to obtain the discrete 2-way envelope delay spectrum. The distorted clean pulse used by the deconvolution algorithm is measured by connecting the two ports of the VNA directly [35]. The amplitude $A(\tau)$ of the delay profile after deconvolution, at time delay τ, is shown by the stem plot in Fig. 4. The received signal at the reader, $\tilde{R}(\tau)$, can be written as (13):

$$\begin{aligned} \tilde{R}(\tau) &= \sum_n A_n(\tau) \\ &\approx R_o \exp\left(-j\overline{\Delta\varphi}\right) \exp\left(-j2\pi f \tau\right). \end{aligned} \tag{15}$$

The mean delay $\overline{\tau}$ of the multipath channel can be calculated by:

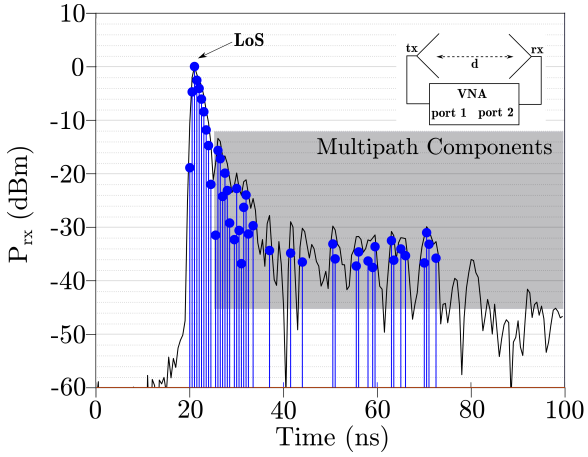

Fig. 4: Solid line: 2-way envelope delay spectrum of the multipath-rich indoor environment (time span: 100 ns, distance d: 3 m between reader and tag antennas). The LoS and the multipath effects are highlighted. Stem plot: the CLEAN algorithm reconstruction of the 2-way envelope delay spectrum. The average time delay $\overline{\tau}$ = 25.0 ns, due to multipath corresponds. Inset: setup used to estimate the multipath effects of the indoor scenario. VNA settings: center frequency 5.8 GHz; span 2 GHz; d = 3 m; # of points 1601; avg.: 16.

$$\overline{\tau} = \frac{\int_0^\infty \tau A(\tau)}{\int_0^\infty A(\tau)}. \tag{16}$$

Although in a multipath-free environment a time delay τ of 20 ns is expected at 3 m, as the leading pulse implies, the presence of multipath adds further delays that shift the average $\overline{\tau}$ to 25.0 ns as computed through (16) and shown in Fig. 4. This corresponds to a positioning error of 37.5 cm according to Table I. Multipath, in fact, is one of the major sources of error, its procedures are not practical for realistic applications because of its complexity and because its accuracy is prone to every environmental changes. Nonetheless, its effects can be mitigated by calibrating the system with measurements at distances above the meter (*e.g.*: at 5 m, Sec. V-C) so that the effects of multipath are taken into account and lower distance estimation errors occur.

IV. The Experimental Setup

Sec. II-C has described a positioning method that uses the received signal phase to estimate, through (7), the distance $\hat{d}$ between the reader and the tag. An experimental setup (Fig. 5a) has been used to test how the phase-based method improves the estimation of tag positioning both for short and long-ranges in indoor and outdoor environments. The benefits of system calibrations are also investigated.

As shown in Fig. 5b and 5c, indoor and outdoor experiments were done while using both Semi-passive ($M \leq 1$) and tunneling tags ($M > 1$). The RF reader (described in [36], [37]) was programmed to operate at 5.8 GHz ISM band, hopping between 50 pre-programmed frequency channels and connected to transmit and receive microstrip patch antennas with a gain $G_{tx,rx}$ = 7.5 dBi and located 1.14 meters above the ground. The transmit power of the reader, P_T, was set

This article has been accepted for publication in a future issue of this journal, but has not been fully edited. Content may change prior to final publication. Citation information: DOI 10.1109/JRFID.2020.3041419, IEEE Journal of Radio Frequency Identification

to 3 dBm to trigger enough gain in the tunneling tag [24]. The signal received by the reader was demodulated and down-converted to base-band, but no base-band amplification was used. The received signal was processed in GNU Radio and MATLAB to extract the phase and amplitude of the received square wave. An FFT filter increases the signal to noise ratio and mitigates the errors due to both phase and thermal noises. A summary of the experimental setups is reported in Tab. II.

Both indoor and outdoor tests were performed. For fair comparison the same patch antenna array with $G_t = 9$ dBi[2] was used on both tags and the LoS distance d from the reader was changed from 5 to 35 meters, with a step width of 5 meters. The reader was programmed for hopping between 50 frequency channels (from 5.75 GHz to 5.8 GHz) with a dwell time of 2 seconds at uniform intervals of 1 MHz (d_{max} = 150 m). The semi-passive tag was modulated by binary phase shift keying (BPSK) with a maximum modulation factor M of -6 dB[3], while the tunneling tag used On-off Keying and, through tunneling, it amplified the backscattered signal ($M > 5$ dB).

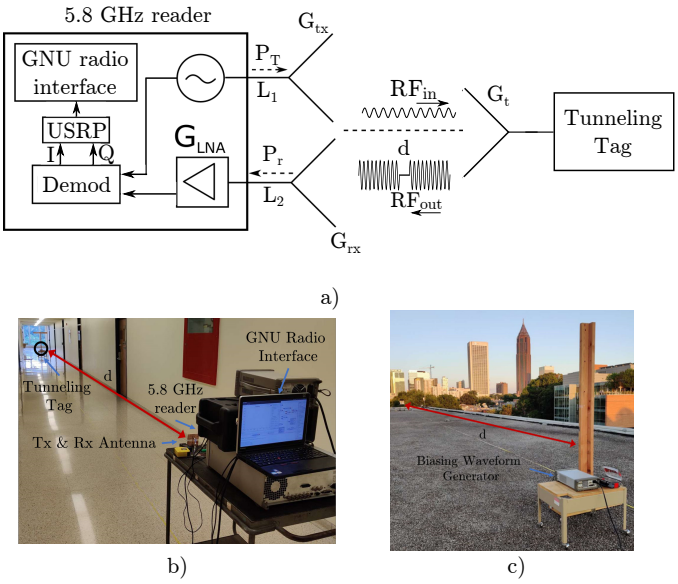

Fig. 5: a) Reader and tag configuration used for indoor and outdoor measurements. $G_{tx} = G_{rx} = 7.5$ dBi, $G_t = 9$ dBi, $P_T = 3$ dBm, $d \in [5, 35]$ m. Photos of the b) indoor and c) outdoor setups used for long range tests.

TABLE II: Specifications of the Experimental Setup

G_t (dBi)	9
d (m)	[5:5:35]
P_T (dBm)	3
$G_{tx,rx}$ (dBi)	7.5
Freq. hopping (GHz)	5.75:5.8
Freq. step Δf (MHz)	1

[2]An array antenna was chosen to allow the Sempi-passive tag to backscatter from longer distances and enable a comparison with the long-range backscattering of the tunneling tag.

[3]Due to internal losses within the on-board RF switch.

V. Experimental Results

A. Exploiting RSP Data

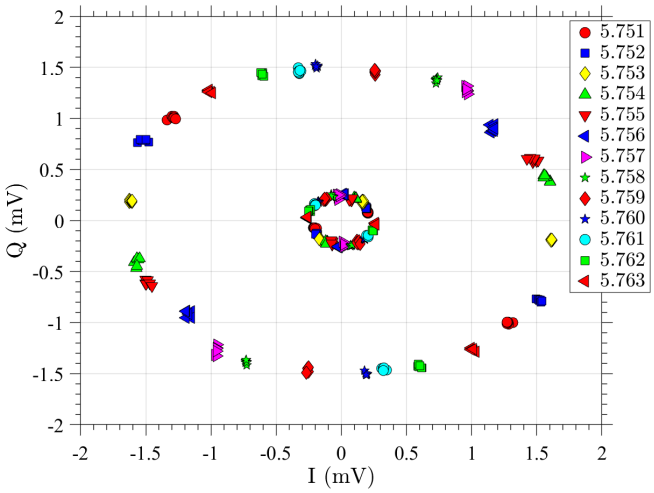

Fig. 6: The IQ constellation points in the 5.8 GHz band (5.751 to 5.763 GHz) for both the Semi-passive and the tunneling tags measured indoor at a distance of 5 m from the reader. The tunneling tag provides a higher level of backscattered power.

The experimental setup detailed in Sec. IV collected the IQ constellations of the received signals for both the Semi-Passive and the tunneling tags at a distance of 5 m away from the reader (impinging power on tag of -42.20 dBm). Fig. 6 shows the received I_{rx} and Q_{rx} values of 13 out of 50 adjacent channels for both the Semi-passive and the tunneling tags; it highlights that the P_{RSS} of the former is 20 dB below the P_{RSS} of the latter. Considering that the tunneling tag has higher gains when the impinging power decreases (especially below -60 dBm), intelligible received powers P_r are expected at longer distances [24].

Fig. 7a illustrates the absolute wrapped phases φ_{RSP} of the received signals while the phase differences between adjacent channels, $\Delta\varphi_{RSP_n} = \left|\varphi_{RSP_n} - \varphi_{RSP_{n+1}}\right|$, are shown in Fig. 7b. When a tag is 5 meters away from the reader, the expected phase difference between two adjacent channels is $\Delta\varphi_{RSP_0} = \frac{4\pi d}{\lambda_e}$ = 0.21 *rad* (12°), with $\lambda_e = \frac{c}{\Delta f} =$ 300 m. Nevertheless, Fig. 7b shows that the phase differences between adjacent channels are generally higher than 12° in both tags due to the combined effects of multipath and wave propagation within the reader. In fact, computing (8) over all the available 50 channels, returns an average phase differences $\overline{\Delta\varphi}$ of 13.27° and 14.33° to which corresponds, through (7), estimated distances $\hat{d}_{SpT}$ = 5.53 m and $\hat{d}_{TT}$ = 5.97 m, for a Semi-passive Tag and a Tunneling Tag, respectively.

Among the three error sources in (11), the one caused by RF cables (ϵ_0) is universal across all distances when using the same hardware setup. Thus, it can be calibrated out by using one or more reference measurements. As reference, therefore, the measurements done on the rooftop (Fig. 5c) were used for both the Semi-passive and the tunneling tags. If the measurement at 1 m is used as reference, then the signal-to-noise ratios are high enough to allow neglecting ϵ_t brought by

This article has been accepted for publication in a future issue of this journal, but has not been fully edited. Content may change prior to final publication. Citation information: DOI 10.1109/JRFID.2020.3041419, IEEE Journal of Radio Frequency Identification

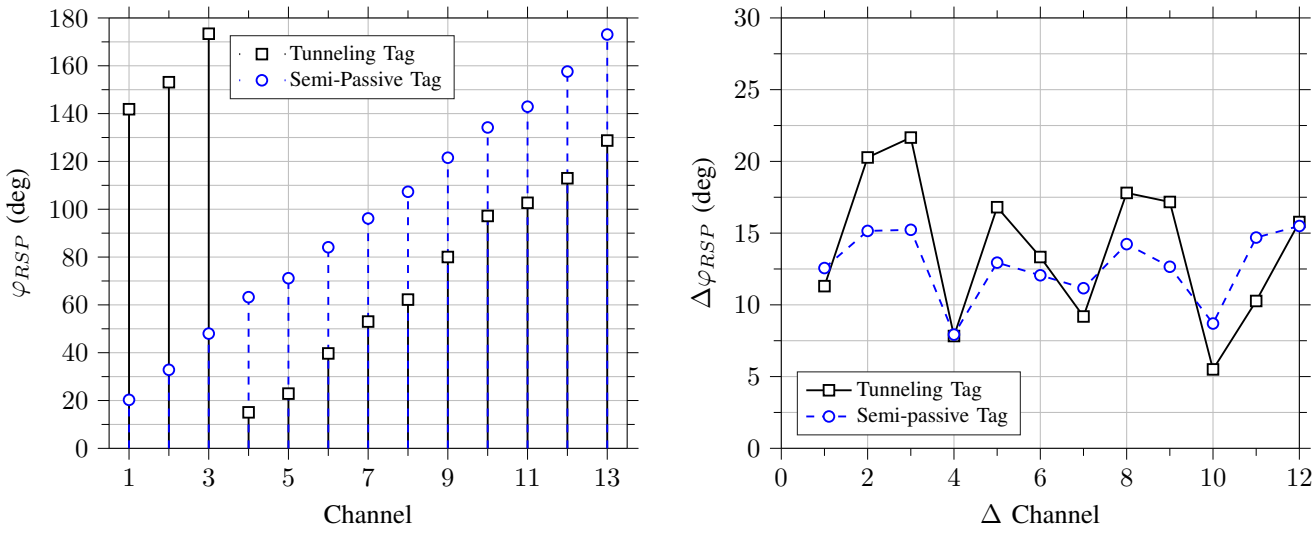

Fig. 7: a) Phases, and b) phase-differences between 13 adjacent channels measured indoor at 5 meters away from the reader for both the Semi-passive (○) and the tunneling tags (□).

the thermal noise. Moreover, both the open environment and the short distance allow to neglect the effects of multipath ϵ_m. The total distance error at 1 m thus becomes:

$$\epsilon_{1m} = \epsilon_0 = \hat{d} - d. \tag{17}$$

If the reference measurement is taken at 5 m instead, all the error sources can be taken into account, thus giving:

$$\epsilon_{5m} = \epsilon_0 + \epsilon_m + \epsilon_t = \hat{d} - d. \tag{18}$$

Calibration at distances higher than 1 m should, therefore, be able to take into account more error sources and provide better accuracy.

B. RSS- vs RSP-based Method

Using the experimental setup described in Sec. IV, the P_{RSS} of both the Semi-passive and the tunneling tags were measured, through (2), when changing their distance d from the reader. Fig. 8a and 8b compare the RSS when using a semi-passive and a tunneling tag; the results clearly show that a semi-passive tag cannot be detected for distances above 15 meters (indoor) and 20 meters (outdoor), while the tunneling tag can still be read at 35 meters, or more, from the reader. Moreover, the measured P_{RSS} of the tunneling tag show a non-linear relationship with the distances because the actual reflection gain depends both on the biasing voltage level, the operating frequency, and the impinging RF power level [22].

RSS-based methods estimate the distance from the reader by inverting the free-space link budget equation in (1) and by substituting P_r with the measured P_{RSS}. Fig. 8c and 8d show the estimated distance $\hat{d}$ for the two types of tags[4] in indoor and outdoor environments and compare them with the estimations obtained through the RSP-based method in (7) *when using measurements taken at 5 meters as calibration data*. The figures highlight how the accuracy of the RSS-based method worsen when the distances increase since multipath significantly affects the received signal power level P_{RSS}. The RSP-based method, on the other hand, significantly improves the positioning accuracy for both semi-passive tags and tunneling tags that operate at longer distances.

Finally, Fig. 9a and 9b show the distance errors ϵ of both RSS- and RSP-based methods for semi-passive and tunneling tags. In both indoor and outdoor measurements, the RSS-based method does not give an accurate estimation when the distance increases, while the RSP-based method provides more accurate results at any distance. For both tags, the RSP-based method can reduce the estimation distance error by at least an order of magnitude at all distances. In fact, the RSS-based method, combined with tunneling tags, gives an average distance error $\bar{\epsilon}$ of 40.6% (9.68 m) and 22.9% (4.71 m) indoor and outdoor, respectively. The proposed RSP-based method, instead, gives a mean error $\bar{\epsilon}$ of 0.8% (0.25 m) and 0.6% (0.15 m) indoor and outdoor, respectively. Thus, it increases the accuracy by a factor of 51 and 38 for the two scenarios.

C. Calibration with Reference Measurements

It is interesting to compare the effects of calibration on the final results of the proposed RSP-based method. For this purpose, Fig. 10a and 10b are used to compare the distance errors ϵ for indoor and outdoor cases when either i) no calibration; or ii) calibration at 1 m; or iii) calibration at 5 m are applied. For each set of data, the average distance error $\bar{\epsilon}$ associated with positioning of the tunneling tag decreases from 1.17 m (no calibration) to 0.65 m (calibration at 1 meter), and up to 0.25 m (calibration at 5 meters) for the indoor tests. It decreases from 0.67 m (no calibration) to 0.22 m (calibration at 1 meter) and up to 0.15 m (calibration at 5 meters) for the

[4]Since the gain of the tunneling tag is difficult to predict at a specific distance, its distance from the reader using the link budget equation was computed by assuming a uniform gain (≈ 18 dB) across all the considered positions.

This article has been accepted for publication in a future issue of this journal, but has not been fully edited. Content may change prior to final publication. Citation information: DOI 10.1109/JRFID.2020.3041419, IEEE Journal of Radio Frequency Identification

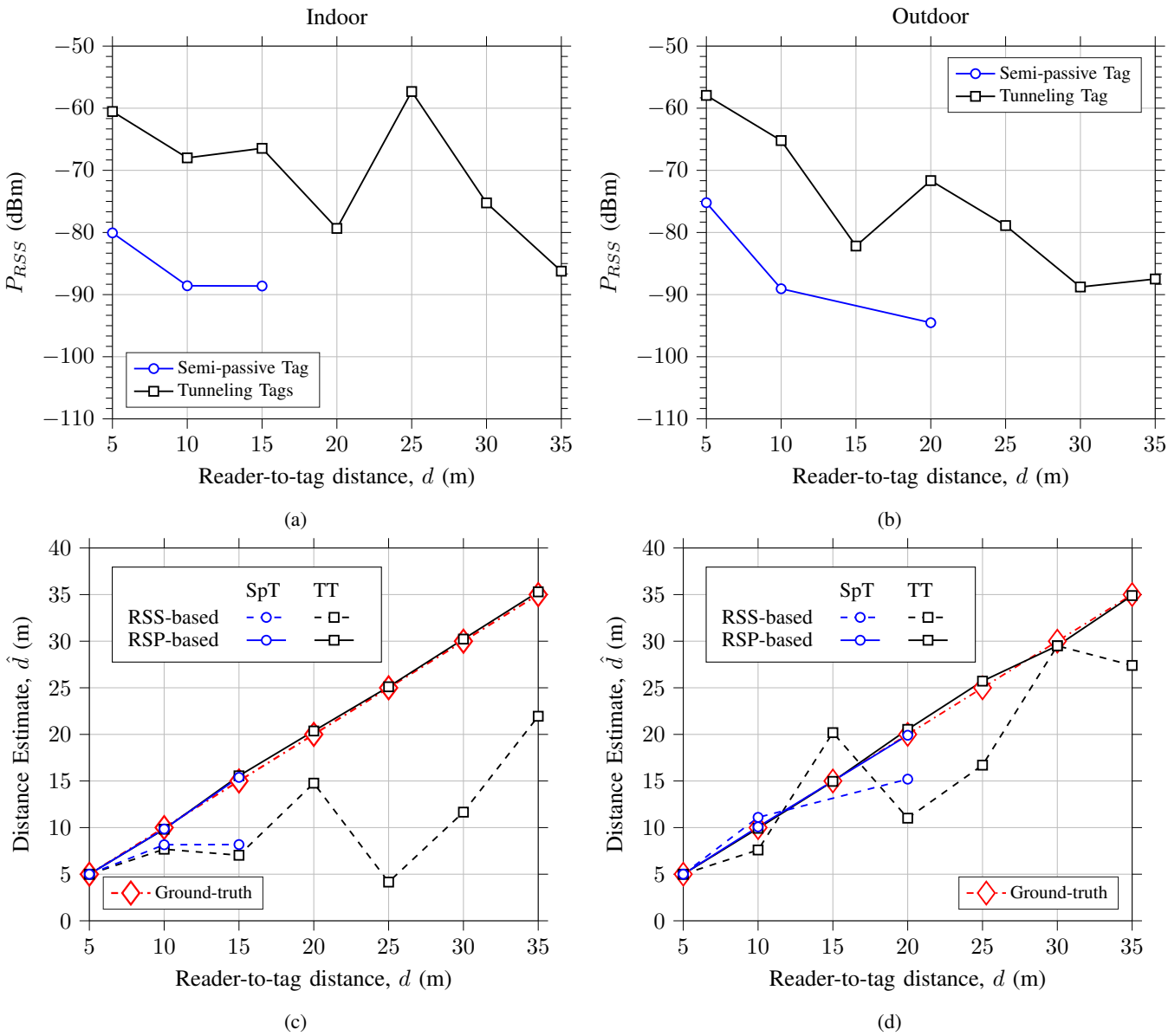

Fig. 8: a) Indoor, and b) outdoor calculated (dashed) and measured (solid) P_{RSS} values. c) indoor, and d) outdoor distance estimates $\hat{d}$ using RSS-based method (dashed) and RSP-based method (solid). Data points are for both Semi-passive (○), and tunneling tags (□).

outdoor tests. Indoor, the estimated distance errors differ by 40 cm according to the type of calibration used (at 1 m *vs* 5 m) since multipath is taken more into account at 5 m. Outdoor, instead, the estimated distance errors differ by only 7 cm.

Positioning within a 35-meter range gives an uncalibrated average distance error $\overline{\epsilon_{\%}}$ of 8.0% and 5.5%, for indoor and outdoor scenarios, respectively. Finally, calibration with reference measurement at 5 m reduces the mean errors to 0.8% and 0.6%, respectively.

Overall, ϵ tends to be constant over the distance with a slight fluctuation in the indoor case where the multipath (ϵ_m) is more significant. The calibration at 5 m applied in an outdoor scenario reduces the average distance error $\overline{\epsilon}$ only from 0.22 m to 0.15 m because of the reduced effect of multipath. The beneficial effect of calibrating the setup at long distances is evident especially for indoor measurements; outdoor, instead, short-range calibrations already provide good accuracy that can be further enhanced by using calibrations at longer ranges.

Considering that an EIRP of 10.5 dBm is used in this work, the maximum reading range can be easily extended up to 1 km by further increasing the EIRP (*e.g.:* an EIRP of 36 dBm used in many unlicensed ISM bands) and by adding base-band amplification in the receiver chain [24]. Since the estimation error does not increase with distance (Fig. 10), a frequency-hopping step Δf of 150 kHz, would increase the maximum range to 1000 m while keeping the same absolute error. Given the $\overline{\epsilon}$ from 0.22 m to 0.15 m, the percentage error $\overline{\epsilon_{\%}}$ at 1000 m can be as low as 0.015% (Fig. 1). At this distance, the range correlation may degrade the phase noise of the LO by maximum 6 dB rather than improving it like

This article has been accepted for publication in a future issue of this journal, but has not been fully edited. Content may change prior to final publication. Citation information: DOI 10.1109/JRFID.2020.3041419, IEEE Journal of Radio Frequency Identification

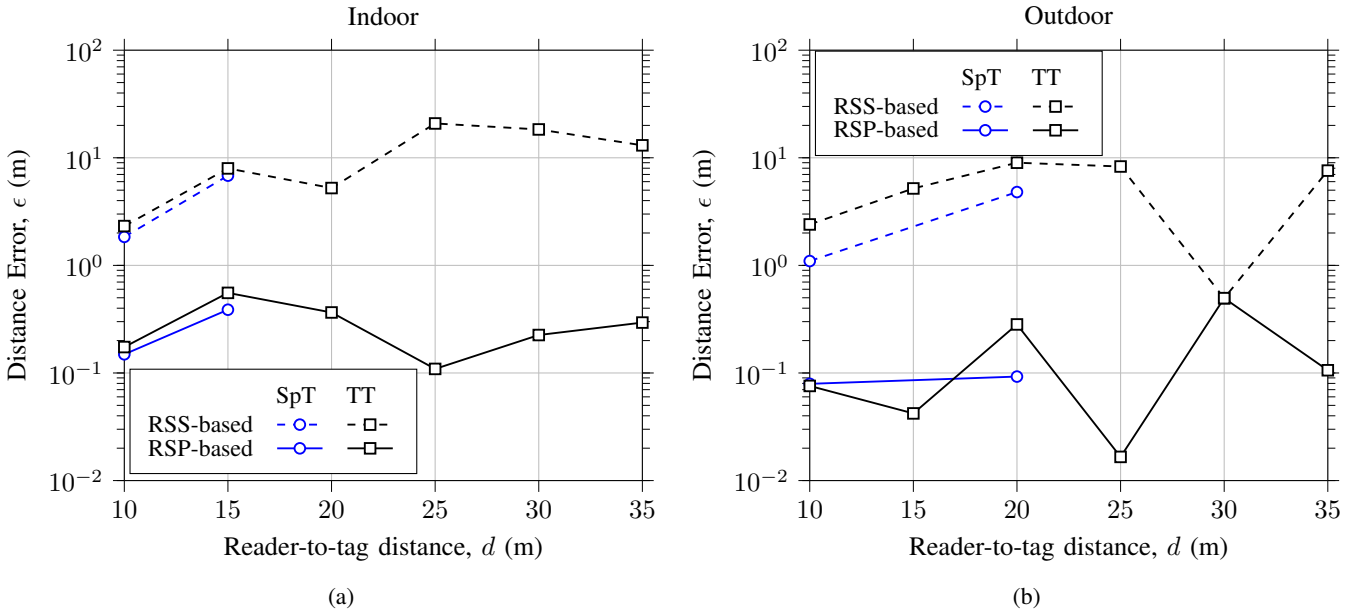

(a) (b)

Fig. 9: a) Indoor, and b) outdoor distance errors ϵ for RSS-based (dashed) and RSP-based (solid) methods with calibration at 5 meters. Data points are for both Semi-passive (○), and tunneling tags (□).

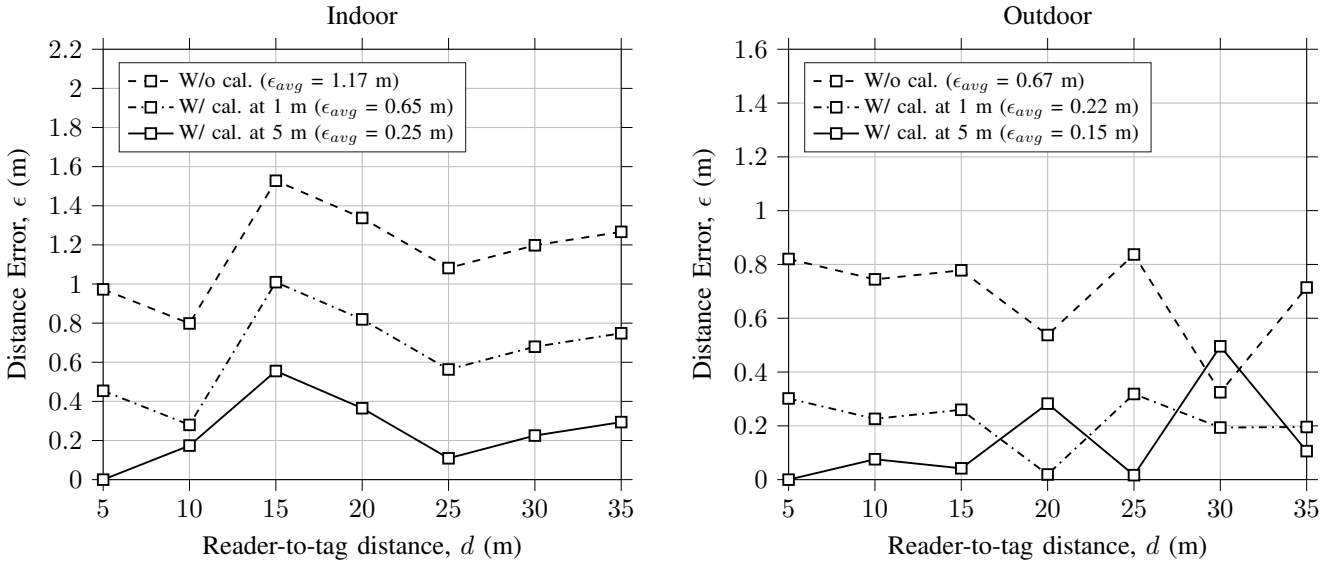

(a) (b)

Fig. 10: Estimated errors ϵ and averages ϵ_{avg} with and without calibrations in a) indoor, and b) outdoor environments for the tunneling tag (□).

at shorter distances [38]. However, after degradation, the LO phase noise of a disciplined commercial oscillator will still satisfy the phase noise requirements of an RFID reader [39].

VI. Conclusions and Future Work

An RSP-based positioning technique has been described and validated for long-range backscattering. Since tunneling tags allow long communication distances, they have been used to prove the proposed method. With appropriate calibration, correct positioning is possible even in a multipath-rich indoor environment. Comparisons with RSS-methods have shown how the RSP-method improves the accuracy by a factor of up to 51. All the results were compared with those of a conventional semi-passive tag; despite the accurate estimation of its position, it proved to have a shorter detectable range than the tunneling tag. Finally, the low-power consumption and an EIRP of only 10.5 dBm confirms how tunneling tags can extend RFID positioning ranges with lower powers and higher accuracy than any other RFID-based positioning techniques.

A comprehensive study to assess the impact of factors other than multipath in different environments (including non-LoS) can be pursued as future work. Hybrid Inertial Microwave

Reflectometry (HIMR) based on a 5.8 GHz backscatter tunneling tag with a 6-axis accelerometer and gyroscope sensors can be developed [17]. Although the tunneling tag in this work relied on an external power supply, the extremely low biasing voltage and current requirements would allow to use a local solar cell [40] that, at long distances from the reader, will provide enough power. Finally, both 2-D and 3-D localization can be implemented by using multiple readers [19].

REFERENCES

[1] C. Qi, F. Amato, M. Alhassoun, and G. D. Durgin, "Breaking the range limit of RFID localization: Phase-based positioning with tunneling tags," in *2019 IEEE International Conference on RFID (RFID)*, April 2019, pp. 1–8.

[2] S. Park and S. Hashimoto, "An intelligent localization algorithm using read time of RFID system," *Advanced Engineering Informatics*, vol. 24, no. 4, pp. 490 – 497, 2010, construction Informatics. [Online]. Available: http://www.sciencedirect.com/science/article/pii/S1474034610000285

[3] D. Boontrai, T. Jingwangsa, and P. Cherntanomwong, "Indoor localization technique using passive RFID tags," in *2009 9th International Symposium on Communications and Information Technology*, Sep. 2009, pp. 922–926.

[4] D. Arnitz, K. Witrisal, and U. Muehlmann, "Multifrequency continuous-wave radar approach to ranging in passive UHF RFID," *IEEE Transactions on Microwave Theory and Techniques*, vol. 57, no. 5, pp. 1398–1405, May 2009.

[5] C. Zhou and J. D. Griffin, "Phased-based composite ranging for backscatter RF tags: System analysis and measurements," *IEEE Transactions on Antennas and Propagation*, vol. 66, no. 8, pp. 4202–4212, Aug 2018.

[6] A. Motroni, P. Nepa, A. Buffi, and B. Tellini, "A phase-based method for mobile node localization through uhf-rfid passive tags," in *2019 IEEE International Conference on RFID Technology and Applications (RFID-TA)*, 2019, pp. 470–475.

[7] X. Yinggang, K. JiaoLi, W. ZhiLiang, and Z. Shanshan, "Indoor location technology and its applications base on improved LANDMARC algorithm," in *2011 Chinese Control and Decision Conference (CCDC)*, May 2011, pp. 2453–2458.

[8] M. Bouet and G. Pujolle, "L-VIRT: Range-free 3-D localization of RFID tags based on topological constraints," *Computer Communications*, vol. 32, no. 13, pp. 1485 – 1494, 2009. [Online]. Available: http://www.sciencedirect.com/science/article/pii/S014036640900111X

[9] L. M. Ni, , , and A. P. Patil, "LANDMARC: indoor location sensing using active RFID," in *Proceedings of the First IEEE International Conference on Pervasive Computing and Communications, 2003. (PerCom 2003).*, March 2003, pp. 407–415.

[10] H. Jiang, C. Peng, and J. Sun, "Deep belief network for fingerprinting-based rfid indoor localization," in *ICC 2019 - 2019 IEEE International Conference on Communications (ICC)*, 2019, pp. 1–5.

[11] S. Azzouzi, M. Cremer, U. Dettmar, R. Kronberger, and T. Knie, "New measurement results for the localization of UHF RFID transponders using an angle of arrival (AoA) approach," in *2011 IEEE International Conference on RFID*, April 2011, pp. 91–97.

[12] M. Cremer, U. Dettmar, C. Hudasch, R. Kronberger, R. Lerche, and A. Pervez, "Localization of passive UHF RFID tags using the AoAct transmitter beamforming technique," *IEEE Sensors Journal*, vol. 16, no. 6, pp. 1762–1771, March 2016.

[13] R. Psiuk, A. Müller, T. Dräger, I. Ibrahim, H. Brauer, H. Töpfer, and A. Heuberger, "Simultaneous 2D localization of multiple coils in an LF magnetic field using orthogonal codes," in *2017 IEEE SENSORS*, Oct 2017, pp. 1–3.

[14] K. Chawla, C. McFarland, G. Robins, and C. Shope, "Real-time RFID localization using RSS," in *2013 International Conference on Localization and GNSS (ICL-GNSS)*, June 2013, pp. 1–6.

[15] D. A. Savochkin, "Simple approach for passive RFID-based trilateration without offline training stage," in *2014 IEEE RFID Technology and Applications Conference (RFID-TA)*, Sep. 2014, pp. 159–164.

[16] Y. Ma, C. Tian, and Y. Jiang, "A multitag cooperative localization algorithm based on weighted multidimensional scaling for passive uhf rfid," *IEEE Internet of Things Journal*, vol. 6, no. 4, pp. 6548–6555, 2019.

[17] M. Akbar, D. Taylor, and G. Durgin, "Hybrid inertial microwave reflectometry for mm-scale tracking in RFID systems," *IEEE Trans. Wireless Comm.*, vol. 14, no. 12, pp. 6805–6814, Dec 2015.

[18] Q. Yang, D. G. Taylor, and G. D. Durgin, "Kalman filter based localization and tracking estimation for HIMR RFID systems," in *2018 IEEE International Conference on RFID (RFID)*, April 2018, pp. 1–5.

[19] M. B. Akbar, "Hybrid inertial microwave reflectometry for mm-scale tracking in RFID systems," Ph.D. dissertation, Georgia Institute of Technology, Atlanta, 2016.

[20] P. V. Nikitin, R. Martinez, S. Ramamurthy, H. Leland, G. Spiess, and K. V. S. Rao, "Phase based spatial identification of UHF RFID tags," in *2010 IEEE International Conference on RFID (IEEE RFID 2010)*, April 2010, pp. 102–109.

[21] C. Zhou and J. D. Griffin, "Accurate phase-based ranging measurements for backscatter RFID tags," *IEEE Antennas and Wireless Propagation Letters*, vol. 11, pp. 152–155, 2012.

[22] F. Amato, C. W. Peterson, B. P. Degnan, and G. D. Durgin, "Tunneling RFID tags for long-range and low-power microwave applications," *IEEE Journal of Radio Frequency Identification*, vol. 2, no. 2, pp. 93–103, June 2018.

[23] M. Alhassoun, M. A. Varner, and G. D. Durgin, "Design and evaluation of a multi-modulation retrodirective RFID tag," in *2018 IEEE International Conference on RFID (RFID)*, April 2018, pp. 1–8.

[24] F. Amato, H. M. Torun, and G. D. Durgin, "RFID backscattering in long-range scenarios," *IEEE Transactions on Wireless Communications*, vol. 17, no. 4, pp. 2718–2725, April 2018.

[25] G. Koo, "Signal constellation of a retrodirective array phase modulator," Master's thesis, Georgia Institute of Technology, Elect. and Comp. Eng., Atlanta, GA, 2011.

[26] J. Cespedes, F. Giuppi, A. Collado, and A. Georgiadis, "A retrodirective UHF RFID tag on paper substrate," in *2012 IEEE International Conference on RFID-Technologies and Applications (RFID-TA)*, Nov 2012, pp. 263–266.

[27] M. M. Islam, K. Rasilainen, S. K. Karki, and V. Viikari, "Designing a passive retrodirective wireless sensor," *IEEE Antennas and Wireless Propagation Letters*, vol. 16, pp. 1739–1742, 2017.

[28] L. C. Van Atta, "Electromagnetic reflector," U.S. Patent 2 908 002, Oct. 6, 1959.

[29] J. Griffin and G. Durgin, "Complete link budgets for backscatter-radio and RFID systems," *Antennas and Propag. Magazine, IEEE*, vol. 51, no. 2, pp. 11–25, Apr. 2009.

[30] F. Amato, C. W. Peterson, M. B. Akbar, and G. D. Durgin, "Long range and low powered RFID tags with tunnel diode," in *2015 IEEE International Conference on RFID Technology and Applications (RFID-TA)*, Sept 2015, pp. 182–187.

[31] G. Durgin, C. Valenta, M. Akbar, M. Morys, B. Marshall, and Y. Lu, "Modulation and sensitivity limits for backscatter receivers," in *Proc. IEEE RFID Int. Conf.*, Apr. 2013, pp. 124–130.

[32] G. Durgin, *Space-Time Wireless Channels*. Upper Saddle River, NJ: Pearson, 2003.

[33] J. Högbom, "Aperture synthesis with a non-regular distribution of interferometer baselines," *Astronomy and Astrophysics Supplement Series*, vol. 15, p. 417, 1974.

[34] T. C. . Liu, D. I. Kim, and R. G. Vaughan, "A high-resolution, multi-template deconvolution algorithm for time-domain UWB channel characterization," in *2007 Canadian Conference on Electrical and Computer Engineering*, April 2007, pp. 1183–1186.

[35] R. G. Vaughan and N. L. Scott, "Super-resolution of pulsed multipath channels for delay spread characterization," *IEEE Transactions on Communications*, vol. 47, no. 3, pp. 343–347, 1999.

[36] C. Qi, J. D. Griffin, and G. D. Durgin, "Low-power and compact microwave RFID reader for sensing applications in space," in *2018 IEEE International Conference on RFID Technology Application (RFID-TA)*, Sept 2018, pp. 1–6.

[37] C. Qi, R. W. Corless, J. D. Griffin, and G. D. Durgin, "Low-power and compact frequency hopping RFID reader at 5.8 GHz for sensing applications in space," *IEEE Journal of Radio Frequency Identification*, vol. 3, no. 3, pp. 133–142, Sep. 2019.

[38] M. C. Budge and M. P. Burt, "Range correlation effects on phase and amplitude noise," in *Proceedings of Southeastcon '93*, April 1993, pp. 5 p.–.

[39] E. Ngompe, "Computing the LO phase noise requirements in a GSM receiver," *Applied Microwave & Wireless*, pp. 54–58, July 1999.

[40] IXYS, "IXOLAR high efficiency solarBIT." Accessed Oct 18, 2020. [Online]. Available: https://ixapps.ixys.com/DataSheet/KXOB22-04X3F_Nov16.pdf

Cheng Qi received the B.S. (2014) and M.S. (2015) degrees from Tianjin University and Georgia Institute of Technology. In 2015, he joined the Propagation Group at Georgia Tech as a graduate research assistant, where he is currently pursuing the Ph.D. degree. His research focuses on antenna design, RFID system design, long-range backscatter communication, space solar power harvesting, and RFID localization technology. He has authored or co-authored more than 12 technical papers and presented his work in multiple international conferences. He received the best paper award for the article presented in the IEEE RFID Conference (2019), and the best student paper award for the paper presented in IEEE RFID-TA Conference (2018). He is a recipient of William C. Brown Fellowship (2017), a winner of the People's Choice Award in NSF Innovation Corps program (2018) in San Francisco, and the winner of first place Ph.D. mentor in Opportunity Research Scholar (ORS) program at Georgia Tech (2018). He has served as a poster session chair and a technical program committee member for IEEE RFID conference since 2018.

Dr. Francesco Amato received the B.S. (2006) and M.S. (2009) degrees in Telecommunication Engineering from the University of Roma Tor Vergata, and the Ph.D. degree in Electrical and Computer Engineering from the Georgia Institute of Technology, Atlanta (USA), in 2017. From 2009 to 2011, he was with SES, Luxembourg, as a Ground System Engineer. In 2015 he was a Research Intern at Intel Labs, Santa Clara, CA. Between 2017 and 2018 he was a Post-Doctoral researcher with the Sant'Anna School of Advanced Studies at the Digital and Microwave Photonics Group, in Pisa (Italy) and a Post-Doctoral Researcher at the Pervasive Electromagnetic Lab of Tor Vergata University in Rome (Italy) in 2019 and 2020. He received, among others, the Fulbright Scholarship in 2012; the Best Student Paper Award of the IEEE International Conference on RFID-Technologies and Applications (RFID-TA) in 2015; the William Brown Fellowship in 2015; the best paper award at the IEEE International Conference on RFID and the Clive Hohberger Technology Award in 2019. He has been member of the organizing committee for the IEEE International Conference on RFID from 2017 to 2020 and serves as Treasurer and Secretary for the IEEE Council of RFID.

Mohammad Alhassoun received the B.Sc. degree in electrical engineering from King Fahd University of Petroleum and Minerals (KFUPM), Saudi Arabia in 2013; the MS; and the PhD degree from the Georgia Institute of Technology, Atlanta in 2015 and 2019, respectively. He is currently an assistant professor at KFUPM. He is the recipient of both the 2018 and 2019 IEEE International Conference on RFID best paper award. He previously worked at Nokia Bell Labs as an EMCD intern and a graduate assistant at KFUPM where he was awarded the best lab instructor in the Department of Electrical Engineering. He was also awarded the Tech to Teaching Certificate in College Teaching from the Georgia Institute of Technology in addition to the Associate Level Certificate from the Center of Integration of Research, Teaching and Learning.

Prof. Gregory D. Durgin joined the faculty of Georgia Tech's School of Electrical and Computer Engineering in Fall 2003 where he serves as a professor. He received the BSEE (96), MSEE (98), and PhD (00) degrees from Virginia Polytechnic Institute and State University. In 2001 he was awarded the Japanese Society for the Promotion of Science (JSPS) Post-doctoral Fellowship and spent one year as a visiting researcher with Morinaga Laboratory at Osaka University. He has received best paper awards for articles coauthored in the IEEE Transactions on Communications (1998 Stephen O. Rice prize), IEEE Microwave Magazine (2014), and IEEE RFID Conference (2016, 2018, 2019). Prof. Durgin authored Space-Time Wireless Channels (2002), the first textbook in the field of space-time channel modeling which has influenced multiple generations of commercial cellular technologies. Prof. Durgin founded the Propagation Group (http://www.propagation.gatech.edu) at Georgia Tech, a research group that studies radiolocation, channel sounding, backscatter radio, RFID, and applied electromagnetics. He is a winner of the NSF CAREER award as well as numerous teaching awards, including the Class of 1940 Howard Ector Outstanding Classroom Teacher Award at Georgia Tech (2007). He has served on the editorial staff for IEEE RFID Virtual Journal, IEEE Transactions on Wireless Communications, and IEEE Journal on RFID. He also serves on Vice-President of Conferences for the IEEE Council of RFID. He is a frequent consultant to industry, having advised many multinational corporations on wireless technology.